THE JOURNAL OF PHYSICAL CHEMISTRY A

Article

pubs.acs.org/JPCA

Direct Dynamics Simulation of the Activation and Dissociation of 1,5-Dinitrobiuret (HDNB)

Rui Sun,[†] Matthew R. Siebert,[†,#] Lai Xu,[†] Steven D. Chambreau,*[,‡] Ghanshyan L. Vaghjiani,[§] Hans Lischka,[†] Jianbo Liu,*[,⊥] and William L. Hase*[,†]

[†]Department of Chemistry and Biochemistry, Texas Tech University, Lubbock, Texas 79409, United States

[‡]ERC Incorporated, Edwards Air Force Base, California 93524, United States

[§]Air Force Research Laboratory, AFRL/RQRP, Edwards AFB, California 93524, United States

[⊥]Department of Chemistry and Biochemistry, Queens College, 65-30 Kissnea Boulevard, Queens, New York 11367, United States

Supporting Information

ABSTRACT: Certain room-temperature ionic liquids exhibit hypergolic activity as liquid bipropellants. Understanding the chemical pathways and reaction mechanisms associated with hypergolic ignition is important for designing new fuels. It has been proposed (*J. Phys. Chem. A* **2008**, *112*, 7816) that an important ignition step for the hypergolic ionic liquid bipropellant system of dicyanamide/nitric acid is the activation and dissociation of the 1,5-dinitrobiuret anion DNB^-. For the work reported here, a quasiclassical direct dynamics simulation, at the DFT/M05-2X level of theory, was performed to model $H^+ + DNB^-$ association and the ensuing unimolecular decomposition of HDNB. This association step is 324 kcal/mol exothermic, and the most probable collision event is for H^+ to directly scatter off of DNB^-, without sufficient energy transfer to DNB^- for H^+ to associate and form a highly vibrationally excited HDNB molecule. Approximately 1/3 of the trajectories do form HDNB, which decomposes by eight different reaction paths and whose unimolecular dynamics is highly nonstatistical. Some of these paths are the same as those found in a direct dynamics simulation of the high-temperature thermal decomposition of HDNB (*J. Phys. Chem. A* **2011**, *115*, 8064), for a similar total energy.

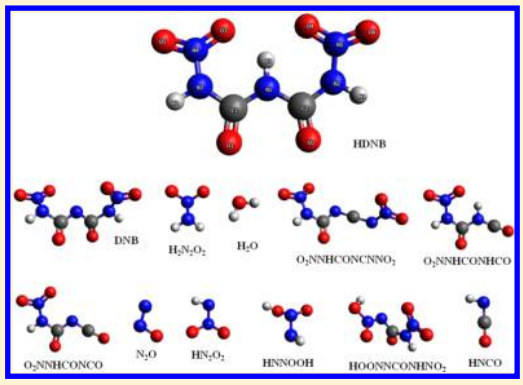

1. INTRODUCTION

Hypergolic ignition involves a spontaneous ignition process of bipropellants (fuel-oxidizer) mixtures at ambient temperature and pressure. It is widely employed for propulsion applications in rocket motors.[1] Ionic liquids exhibit low vapor pressure, high energy density, and high solubility in many polar solvents and are potential fuels and monopropellants.[2] There have been a significant number of studies on the properties of ionic liquid chemistry in the past decade.[3−5] These studies have provided detailed information for investigating reactivity trends and screening for the best ionic liquid candidates for hypergolic ignition. Dicyanamide was chosen not only because it is a fuel-rich anion but also because ionic liquid dicyanamides have some of the lowest viscosities among known ionic liquids,[6−8] making them excellent candidates as bipropellants.

Schneider et al.[9] studied the hypergolic ionic liquid fuel based on the reaction of dicyanamide anions with white fuming nitric acid. According to the mechanism proposed by Chambreau et al.,[10] the association of a proton H^+ with the DNB^- anion to form the HDNB (1,5-dinitrobiuret) molecule is an important initial step in the hypergolic ignition of the dicyanamides anion with white fuming nitric acid.[10] The structures of the DNB^- anion and the HDNB molecule are shown in Figure 1.

It is a challenging problem to establish the atomic-level mechanism for a hypergolic ignition process. The reactions are highly exothermic, heterogeneous and vigorous, with highly reactive intermediates, and are difficult to probe experimentally. Computational studies offer a general approach for considering and testing the possibility of various mechanisms for hypergolic ignition. An illustrative study is that of Izgorodina et al.[11] who used ab initio calculations to study the mechanisms of nucleophilic addition of water and methanol to the dicyanonitrosomethanide anion in the absence of the usual transition-metal promoters. Another computational approach is to use direct dynamics simulations[12,13] and energize the reactants to simulate the experimental conditions. Their reaction dynamics may be followed in time and, thus, the reaction pathways and product molecules could be identified. There is an important discovery element to these simulations in that they may provide new unexpected information regarding possible important reaction and energy dissipation pathways for the hypergolic ignition of fuels. Such studies have the potential

Received: January 9, 2014
Revised: February 17, 2014
Published: February 26, 2014

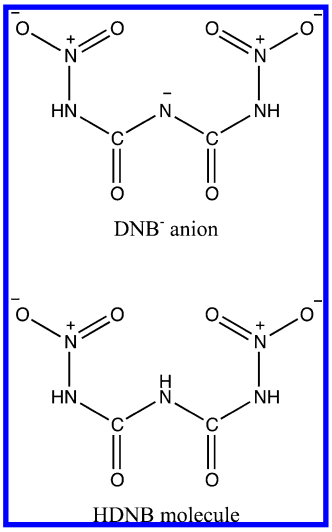

Figure 1. Structures of the DNB^- anion and the HDNB molecule.

of assisting in the development of new and more efficient hypergolic bipropellants.

In previous work, Liu et al.[14] performed quasiclassical direct dynamics trajectory simulations of the thermal decomposition of HDNB molecules. For the 4000−6000 K temperature range, they observed five principal decomposition pathways shown in Table 1. The work presented here builds on this previous study of Liu et al.,[14] and instead of studying the thermal decomposition of HDNB, the decomposition of nonrandomly excited HDNB is studied by a direct dynamics simulation[13] to model H^+ and DNB^- collisions, which form a vibrationally excited HDNB molecule with a nonrandom distribution of internal energy. The ensuing unimolecular decomposition of the molecule is then investigated. H^+ + DNB^- association releases 324 kcal/mol of energy, and there is the potential for localization of this energy in HDNB, promoting nonstatistical decomposition with multiple bonds broken such as N−N, N−C, and N−O bonds. From the NIST database,[15] the N−N, N−C, and N−O bond energies are 38.2, 72.9, and 48.0 kcal/mol, respectively. The large amount of association energy is much higher than the dissociation energies of these bonds, and multiple bond ruptures may occur. The direct dynamics simulation reported here probes these possible dynamics.

2. COMPUTATIONAL METHODS

A. Electronic Structure Calculations and Potential Energy Surface. In previous work, Izgorodina et al.[16] showed that density functional theory (DFT) methods provide accurate ion pair binding energies for ionic liquids. After comparing with benchmark results, their work showed that M05-2X[17,18] is one of the functionals with the highest accuracy.[17] To further test the accuracy of different electronic structure theory methods, as well as their computational cost, we studied the proton affinity for the two binding sites of the model system $H^+ + N(CN)_2^-$. Geometry optimizations were performed and energies calculated for the resulting binding sites using MP2[19] and different DFT functionals with the basis sets 6-31++G**,[20] 6-311++G**,[21] aug-cc-pvdz,[22] and aug-cc-pvtz.[22,23] The DFT functionals included B3LYP,[24] M05-2X,[17,18] BHandH,[25] PBE0,[26] BLYP,[27,28] B1B95,[29] X3LYP,[30] SVWN5,[31,32] and B3-PW91.[24] Table 2 gives the results obtained from these calculations. CCSD(T)[33] single-point calculations were performed based on optimized geometries obtained at different levels of DFT and MP2 theory and are included as benchmark energy values. The energies are quite similar for the different DFT and MP2 calculations and slightly less exothermic than CCSD(T) values. The latter are only weakly sensitive to the method used to obtain the optimized geometries for the single-point calculations.

Of interest for the work presented here is to model the association dynamics of H^+ and DNB^-. In addition to the singlet electronic state for H^+ and DNB^-, the reactants may also be in singlet electronic states for H^- + DNB^+ and the doublet radicals H• + DNB•. For H^+ + DNB^- and H^- + DNB^+, each of the reactants is a singlet. The relative energies of H^- + DNB^+, H^+ + DNB^-, and H• + DNB•, as calculated with M05-2x/6-31++G** theory, are shown in Figure 2. The potential energy curve for H• + DNB• association to form HDNB was modeled by H• + •$N(CH_3)_2$ association and calculated with the open-shell M05-2x/6-31++G** method. At this level of theory, H• and •$N(CH_3)_2$ associate smoothly and adiabatically to $HN(CH_3)_2$, with a classical binding energy of 100.1 kcal/mol. For comparison, the H• + DNB• binding energy is 124.7 kcal/mol with M05-2x/6-31++G**. In Figure 2, the potential energy curve for H• + DNB• association is modeled by scaling the H• + •$N(CH_3)_2$ potential energy curve by the relative H• + DNB• and H• + •$N(CH_3)_2$ association energies, that is, 124.7/100.1. For H^+ + DNB^- association and formation of HDNB, there is an electronic nonadiabatic transition from the potential energy surface (PES) for H^+ + DNB^- to that for H• + DNB• → HDNB. The details of this transition are not considered here, and instead, as discussed below, the trajectories are initiated on the H• + DNB• → HDNB PES, with an excess energy originating from the H^+ + DNB^- → H• + DNB• electronic transition.

B. Direct Dynamics Simulations. In addition to the accuracy, the computational cost is also important for direct dynamics simulations. The software package used for the simulations was VENUS[34,35] interfaced[36] with NWChem.[37] The comparative computational cost in performing a frequency calculation for B3LYP, M05-2X, and MP2 with the 6-31++G** basis set using this code is 1.00, 1.48, and 2.94. Test trajectories were carried out with each of these electronic structure methods, and the actual comparative costs for the simulations were 1.00, 1.51, and 9.65. The much higher cost of the MP2 direct dynamics is uncertain and may arise from the inefficient convergence of the Hartree−Fock calculation, required for the inclusion of electron correlation with MP2. In considering the accuracy, the computational cost, and the previous work of Izgorodina et al.,[17] the open-shell M05-2X/6-31++G** method was chosen for the direct dynamics simulations.

H^+ + DNB^- association was modeled by assuming that a nonadiabatic electronic transition occurs to the H• + DNB• → HDNB PES. The trajectories were initiated as H• + DNB•, and the potential energy released by the H^+ + DNB^- → H• + DNB• electronic transition, (i.e., 198.8 kcal/mol) was assumed to become relative translational energy. Quasiclassical sampling[38] was used to select initial conditions for the H• + DNB• trajectories. The initial separation between H• and DNB• was set at 10 Å, with a collision impact parameter of 0 Å. The vibrational and rotational temperature of DNB is 298 K, and quasi-classical Boltzmann sampling was used to select the vibrational and rotational energies. The DNB molecule was then randomly rotated about its Euler angles. The 198.8 kcal/mol for the H^+ + DNB^- → H• + DNB• electronic transition

Table 1. Five Principal Decomposition Pathways Observed in the Temperature-Dependent Direct Dynamics Simulation of HDNB Decompostion[a]

Path	Decomposition Products	Trajectory Ratios (%)		
		4000K	5000K	6000K
1	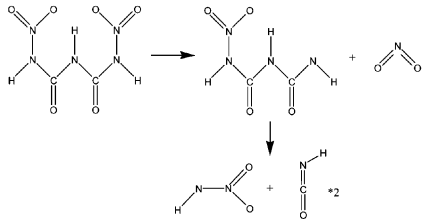	34±6	39±7	43±7
2	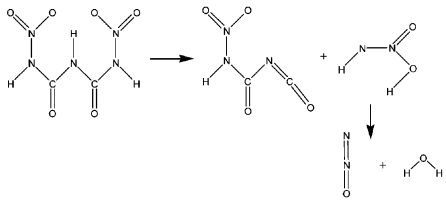	26±6	13±5	7±3
3	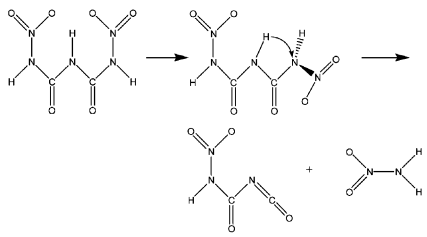	10±4	6±3	4±2
4	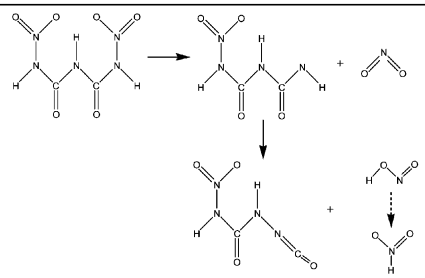	4±2	8±4	10±4
5	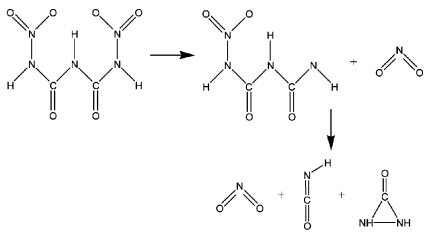	8±4	13±5	26±6
	Sum of other dissociation paths	8±4	21±8	10±4
	Non-reactive	10±4	0	0

[a]Results from ref 14.

was then added as relative translational energy. A total of 300 trajectories were calculated.

For numerical integration of the classical equations of motion, the velocity Verlet[39] and sixth-order symplectic[40,41] algorithms were compared, using time steps of 2.5, 1.0, 0.5, 0.1, and 0.05 fs. After consideration of both energy conservation and computational cost, velocity Verlet with a time step of 0.5 fs was chosen for the simulations. Ensuring that the trajectories remain in the same electronic state during the trajectory is important for an adiabatic direct dynamics simulation, and it is particularly difficult in this case because the system's total energy is very high and the molecular structure may vary greatly during one trajectory integration time step. In the research presented here, not only the initial guess of the molecular

Table 2. $N(CN)_2^- + H^+$ Association Energies for Different Levels of Theory

method	basis set			
	6-31++G**	6-311++G**	aug-cc-pVDZ	aug-cc-pVTZ
		$N(CN)_2^- + H^+ \rightarrow HN(CN)_2$		
B3LYP[a]	−302.9	−302.7 (−315.4)[b]	−302.1	−303.3 (−315.4)
M05-2X	−302.9	−301.3 (−315.3)	−301.5	−303.6
BHandH	−302.0	−301.8	−300.9	−302.3
PBE0	−303.2	−303.1	−302.4	−303.6
BLYP	−300.6	−300.6	−300.1	−301.2
B1B95	−303.8	−303.7	−303.0	−304.4
X3LYP	−289.3	−302.4	−301.7	−303.0
SVWN5	−293.4	−292.9	−292.8	−293.7
B3-PW91	−303.3	−303.1	−302.5	−303.8
MP2	−306.3	−306.7 (−315.3)	−302.8	−304.3 (−315.4)
		$N(CN)_2^- + H^+ \rightarrow (NC)N(CNH)$		
B3LYP[a]	−308.5	−308.2 (−314.4)[b]	−307.5	−310.0 (−314.5)
M05-2X	−304.7	−303.4 (313.8)	−303.7	−310.5
BHandH	−304.7	−304.9	−303.8	−306.3
PBE0	−308.8	−308.8	−308.1	−310.5
BLYP	−308.8	−308.6	−307.9	−310.4
B1B95	−309.2	−309.0	−308.3	−310.8
X3LYP	−294.7	−307.7	−306.9	−309.4
SVWN5	−306.6	−305.7	−305.1	−307.2
B3-PW91	−309.8	−309.7	−309.1	−311.5
MP2	−303.9	−304.2 (−314.1)	−301.3	−306.2 (−314.4)

[a]The energy for B3LYP/6-31+G** is −302.8 kcal/mol for $N(CN)_2^- + H^+ \rightarrow HN(CN)_2$ and −310.4 kcal/mol for $N(CN)_2^- + H^+ \rightarrow (NC)N(CNH)$, adapted from ref 10. [b]The numbers in parentheses are the energies from CCSD(T)/aug-cc-pVTZ at the geometry corresponding to the level of theory.

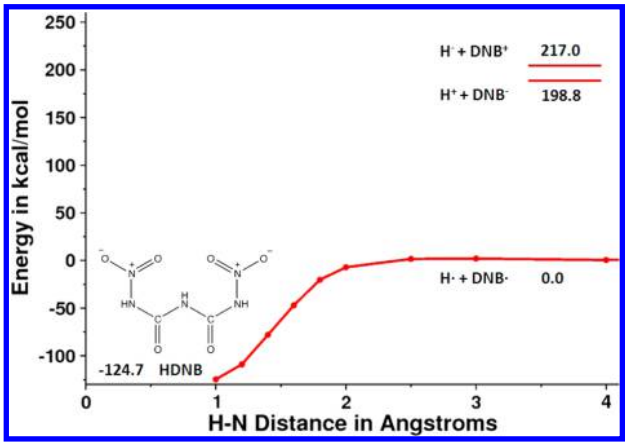

Figure 2. Energies for the H^- + DNB^+, H^+ + DNB^-, and H• + DNB• singlet electronic states and the H• + DNB• → HDNB potential energy curve, which was modeled by scaling the H• + $\bullet N(CH_3)_2$ potential energy curve by the relative H• + DNB• and H• + $\bullet N(CH_3)_2$ association energies.

orbital (MO) for each ab intio calculation was obtained from the previous trajectory point, but also the total energy of the trajectory was checked during the simulation to ensure that the energy fluctuation between every two points was less than 1% of the total energy. A time step of 0.5 fs was chosen for the trajectories, and it was generally small enough for SCF convergence in most of the trajectories as well as to keep the total energy constant. However, for some of the initial conditions, a time step as small as 0.1 fs was required to calculate an accurate trajectory. The trajectories were halted at 1 ps or if two dissociation products were separated by more than 10 Å. Accurate trajectories were calculated for each of the 300 initial conditions.

3. HDNB CONFORMERS AND THEIR PES

Before presenting the results of the direct dynamics simulations, it is worth noting that HDNB may exist in a C_2, C_s, or twisted conformation, with the C_s conformer being the most stable (see Figure 3). The interconversion from C_2 to C_s requires rotating two C−N bonds attached to the same C atom, which is less likely to accomplish via a single transition state (TS); therefore, the twisted conformer acts as an intermediate structure between the C_2 and C_s conformers. Figure 3

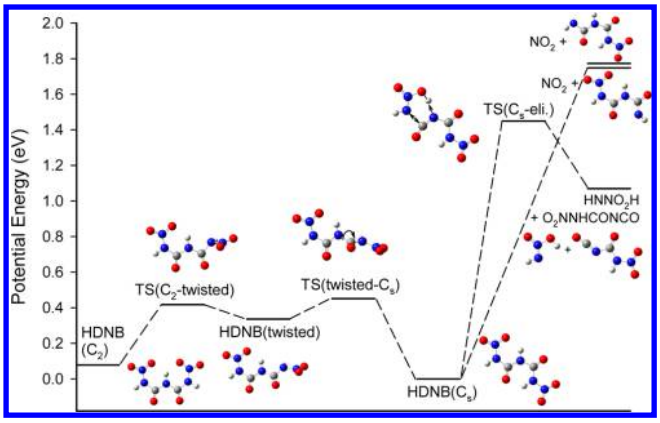

Figure 3. Reaction coordinate for interconversion of various HDNB conformers and subsequent dissociation paths of the C_s conformer. Energies of complexes, TSs, and products, relative to the C_s conformer, are derived from B3LYP/6-31++G(d,p) results, including zero-point energies.

dx.doi.org/10.1021/jp5002622 | J. Phys. Chem. A 2014, 118, 2228−2236

Table 3. Direct Dynamics Trajectory Simulation Results for H• + DNB• Collisons

Path	Trajectory Products	Trajectoy Ratios(%)
1	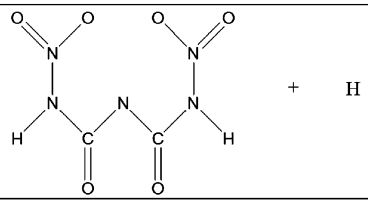	66.7
2	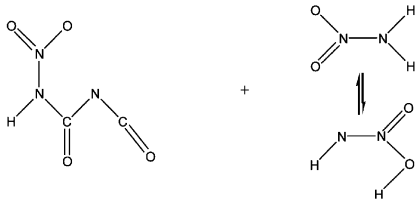	26.0
3	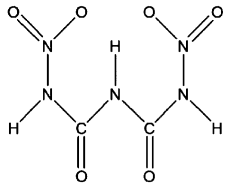	2.7
4	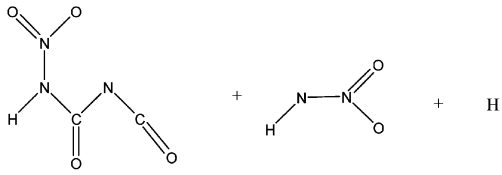	1.7
5	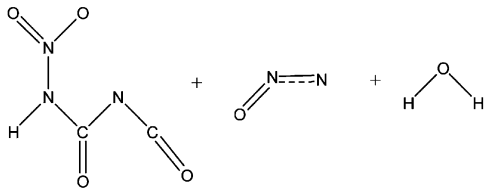	1.0
6	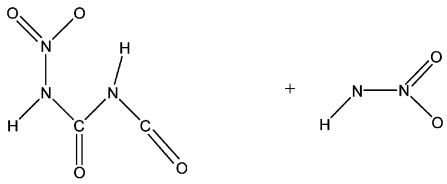	1.0
	Sum of other dissociation paths [a]	1.0

[a]The dissociation paths are described in the text.

summarizes these three conformers and the corresponding TSs involved in the structure interconversion, all of which are calculated at the B3LYP/6-31++G(d,p) level of theory. An energetically favorable interconversion pathway would be HDNB(C_2) → TS(C_2−twisted) → HDNB(twisted) → TS(twisted−C_s) → HDNB(C_s).

At simulation temperatures of 4000−6000 K used in Liu et al.'s study,[14] the HDNB molecule is vigorously excited due to its high internal energy content. Consequently, all energetically accessible conformations of HDNB are expected to be involved in trajectory simulations of HDNB thermal decomposition. Animation of a representative trajectory is provided in the Supporting Information, showing facile interconversions between the HDNB C_2, twisted, and C_s conformations. Statistical interconversions among these conformers occur on a time scale of picoseconds, which is significantly shorter than the HDNB decomposition time scale of nanoseconds or longer. Based on RRKM statistical modeling,[42] the densities of states for the C_2, C_s, and twisted conformations are roughly equal at 750−2000 K. Consequently, for the thermal, statistical decomposition HDNB should be best treated as a mixture of the three different conformers.

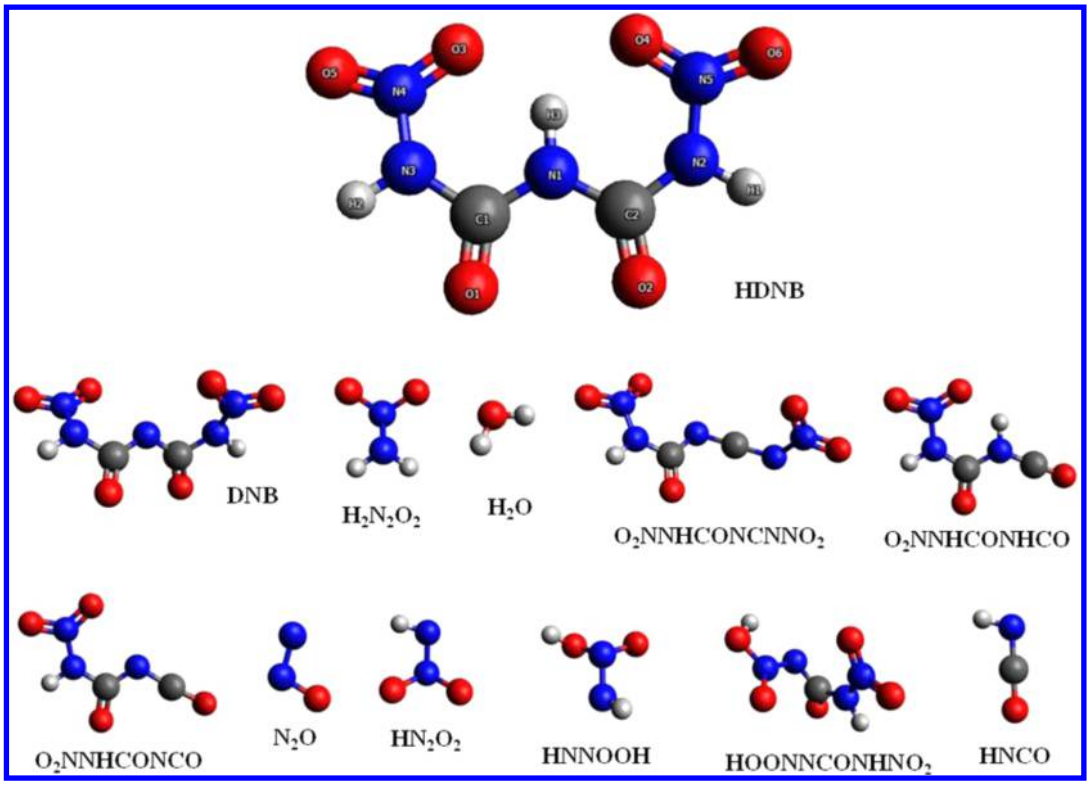

Figure 4. Molecular structures of HDNB and its decomposition products.

In Liu et al.'s article,[14] the reaction coordinate for the initial decomposition of HDNB (shown in Figure 5 of the article) focused on the C_2 and twisted conformers. Figure 3 of the present article has mapped out the reaction coordinate for the C_s conformer, including the TS and stable products using the B3LYP/6-31++G(d,p) method. It is found that the C_2 and C_s conformers have nearly equal 0 K barriers, including zero-point energy to eliminate NO_2 (i.e., 1.73 eV for C_2 and 1.75−1.77 for C_s depending on which terminal $-NO_2$ is lost), and similar energy barriers to eliminate $HNNO_2H$ (i.e., 1.2 eV for C_2 and 1.4 eV for C_s). The corresponding decomposition rate constants are also similar for these two conformers.

For the current H^+ + DNB^- simulations, the total HDNB energy content is similar to that for the thermal decomposition studies of Liu et al. (see section 5).[14] However, for the current simulation, HDNB is excited nonrandomly and not statistically as in the previous thermal simulations, and it is of interest to determine if this nonrandom excitation affects the ensuing dynamics of the HDNB conformers.

4. RESULTS AND DISCUSSION

Eight different reaction pathways were found for the 300 trajectories. Six of the pathways are indentified in Table 3, and the remaining two are discussed below. Molecular structures of HDNB and its decomposition products, observed in the trajectories, are depicted in Figure 4. Only four of the eight paths have percentage yields greater than 2%. The remaining four have percentages of 1% or less. In the following, the atomistic mechanisms for the pathways are described. Animations of these mechanisms are given on the Website http://hase-group.ttu.edu/.

HDNB conformer transitions are only important for path 3, for which HDNB remains intact at the conclusion of the 1 ps trajectories. For the other reaction paths, which form products, conformer transitions for HDNB are very rare. For example, in path 2, conformer transitions only occur for 2 out of the 78 reactive trajectories. Therefore, for all of the reaction pathways that form products, reaction occurs without statistical sampling of the different HDNB conformers.

Path 1, H• + DNB•. There were 200/300 trajectories directly scattered back to the H• + DNB• reactants, with only one inner turning point in the H• + DNB• relative motion. For 59% of these trajectories, the H-atom collided with the central N-atom of DNB, but for each, there was no H−N bond formation and vibration of the H−N bond. To assist in analyzing the trajectories, the time was determined when, during the collision, the distance between the colliding H-atom and the central N-atom of DNB started to increase. The average time required from the initiation of the trajectories at a 10 Å H• + DNB• separation to the above collision distance is 24 ± 0.1 fs. In contrast, the average time required for H• + DNB• to separate from this collision distance to a H• + DNB• separation of 10 Å is 63 ± 1.0 fs. As discussed in the following, the origin of this longer length time is the substantial transfer of the initial H• + DNB• relative translational energy to the DNB• vibrational and rotational energy. Overall, the average time for these direct H• + DNB• unreactive collisions is quite short, that is, 87 fs.

The relative translational energy distribution for the scattered H• + DNB• reactants is given in Figure 5. These relative translational energies vary from 1 to 178 kcal/mol, with an average of 60 kcal/mol. DNB receives a substantial amount of vibrational and rotational energy, and decomposition of DNB is expected for some of the trajectories if they are integrated for a longer period of time.

Path 2, $H_2N_2O_2$ + $O_2NNHCONCO$. There are 78/300 trajectories that result in N3−C1 or N2−C2 bond scission (see Figure 4), which is the major decomposition pathway observed

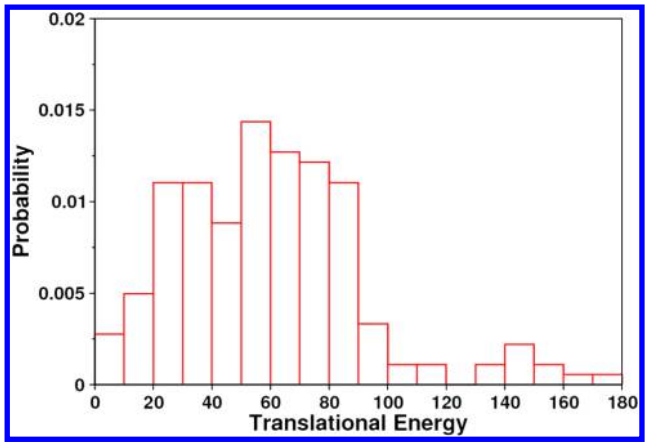

Figure 5. Translational energy (kcal/mol) distribution for the scattered H• + •DNB reactants for path 1.

in the simulations. Instead of scattering off of the DNB molecule as for path 1, the colliding H-atom interacts strongly with the central O1, O2, and N1 atoms of DNB. The H-atom is initially delocalized and moves among these atoms, with frequent isomerizations of the HDNB molecule. The HDNB molecule is highly vibrationally excited because all of the H• + DNB• relative translational energy is transferred to vibrational and rotational energy of HDNB. During intramolecular vibrational energy redistribution (IVR) of this HDNB excitation energy, one of the C−N−N−O_2 chains "wags" toward the center of the molecule, and the "hot" H-atom attaches to either one of the N-atoms of this chain or one of the terminal O-atoms. Then, dissociation of the N3−C1 or N2−C2 bond occurs, leading to the H_2NNO_2/HNNOOH and O_2NNHCONCO products.

As discussed above, this N−C bond dissociation is assumed to have occurred when the N−C bond length exceeded 4 Å. With this definition, the time required to form these N−C dissociation products varied from 92 to 599 fs, with an average time of 166 ± 11.2 fs. Time equal to "zero" for these dissociation times is described above and defined when the distance between the colliding H-atom and the central N-atom first increases.

The H_2NNO_2/HNNOOH product is highly excited, and there are frequent isomerizations between the H_2NNO_2 and HNNOOH structures. As a result of this excitation, 40% of this product underwent secondary dissociations during the 1 ps integration of the trajectories to form the following products: NNO + H_2O (26%); HNO + HNO (4%); H_2 + N_2O_2 (3%); N_2 + H_2O_2 (3%); HNO_2 + HN (3%); OH + N_2OH (1%); and H_2 + N_2 + O_2 (1%). These products are depicted in Figure 4.

Path 3, HDNB. The HDNB molecule was formed from 8/300 trajectories, which did not dissociate during the 1 ps trajectories. All of the reactant H• + DNB• relative translational energy is initially localized in the vicinity of the binding H-atom, which undergoes multiple isomerization reactions, transferring between the central N1 atom and the adjacent O1 and O2 atoms. The frequency of these isomerization reactions decreases as the simulation continues, as a result of IVR, and is replaced by rotations of the NO_2 groups at the termini of HDNB and waggings of the skeleton of HDNB. These dynamics illustrate the transfer of vibrational energy from the initially excited binding H-atom to other vibrational modes of the molecule.

The skeleton of DNB• is twisted, and, therefore, the initially formed HDNB molecule has a structure similar to the HDNB(twisted) structure in Figure 3. Numerous enusing HDNB(C_2) ↔ HDNB(twisted) ↔ HDNB(C_s) conformer transitions are observed through the corresponding TSs.

Path 4, H + HN_2O_2 + O_2NNHCONCO. Here, 5/300 trajectories result in N3−C1 or N2−C2 bond scission as the incoming H-atom directly scatters off of DNB. The collision transfers energy directly to one of the N−C bonds, leading to its dissociation and formation of HN_2O_2.

Path 5, NNO + H_2O + O_2NNHCONCO. These products are formed from 3/300 trajectories. The incoming H-atom forms an H−O bond with a terminal −NO_2 group within 35 fs. The NOONNH group is highly excited, and the O-atom to which the H-atom is attached abstracts the H-atom from N−H, forming H_2O and NNO.

Path 6, HN_2O_2 + O_2NNHCONHCO. Here, 3/300 trajectories followed this pathway, which is similar to path 2. As for path 2, the incoming H-atom first strongly interacts with the middle N-atom and the two adjacent O-atoms, before attaching to an O-atom of the terminal −NO_2 group. However, when N−C scission occurs, the H-atom of the N−H group attaches to the O-atom of this scission, and HN_2O_2 is formed instead of $H_2N_2O_2$ for path 2.

Path 7, H_2O + O_2NNHCONCNNO$_2$. Here, 1/300 trajectories followed this interesting path. The incoming H-atom first strongly interacts with the middle N-atom and the two adjacent O-atoms, but instead of transferring to a terminal NO_2 group, the H-atom binds to one of the O-atoms, and the −OH group is eliminated along with H-atom, forming H_2O.

Path 8, HNCO + HOONNCONHNO$_2$. Here, 1/300 trajectory followed this complex reaction path. The incoming H-atom strongly interacts with the middle N-atom and carbonyl O-atoms, highly energizing this part of the HDNB molecule. As a HNCO group is eliminated, the terminal NO_2 group forms a N−N bond with the central N-atom, and the incoming H-atom transfers to the NO_2 group.

5. COMPARISON WITH PREVIOUS DIRECT DYNAMICS SIMULATIONS

It is of interest to compare the current direct dynamics simulations with those reported previously by Liu et al.[14] These two simulations have addressed different conditions for dissociation of HDNB. Liu et al. consider conditions for which the ionic liquid is fully thermally equilibrated. In contrast, the current study considers a possible initiation step, before thermal equilibrium is attained, for which a proton associates with the DNB$^-$ anion, that is, a highly nonequilibrium process forming an excited HDNB molecule with a nonrandom and nonthermal vibrational energy distribution. In addition, different electronic structure theory methods were used for the two simulation studies. Liu et al.[14] used restricted B3LYP/6-31G* for their simulations, while the current simulations were performed with open-shell M05-2X/6-31++G** theory.

For the work of Liu et al.,[14] the quantum number n_i of ith HDNB vibrational mode is sampled using the quantum Boltzmann probability distribution

$$P(n_i) = \exp\left(\frac{-n_i h\nu_i}{k_B T}\right)\left[1 - \exp\left(\frac{-h\nu_i}{k_B T}\right)\right] \quad (1)$$

where ν_i is the vibrational frequency of the ith mode and T is the HDNB temperature. Rotational energy was added by

sampling the classical Boltzmann distribution.[38] The simulations were performed for temperatures of 4000, 5000, and 6000 K, for which the average HDNB energies above the HDNB zero-point energy level (i.e., 62 kcal/mol) are 294, 379, and 464 kcal/mol, respectively. In contrast, for the current simulations, the total energy is 330 kcal/mol above the DNB• zero-point energy of 58 kcal/mol. With zero-point energies included, the respective average energies of the 4000, 5000, and 6000 K simulations are 92, 114, and 136% of that for our simulation of H^+ + DNB^- association. Thus, overall, the two simulation studies have similar total energies.

There are both similarities and differences between the two simulations. Path 2, including the dissociation of the $H_2N_2O_2$/HNNOOH product observed in the current simulations is the same as paths 2 and 3 in the work of Liu et al. For the current study, 26% of the trajectories followed this pathway, while for the work of Liu et al.,[14] 36, 19, and 11% followed this pathway at 4000, 5000, and 6000 K, respectively. The most important path in the work of Liu et al., that is, their path 1, is not observed in the current study. Apparently, neither the H• + •DNB association step or IVR "puts" energy in the correct HDNB vibrational modes to promote Liu et al.'s path 1. In addition, paths 4 and 5 found by Liu et al. were not observed in the current study, and paths 4−6 for the current study were not found by Liu et al.[14] These comparisons show that the nature of HDNB excitation, that is, thermal/random or nonrandom by H• + •DNB association, has a pronounced effect on its unimolecular dissociation dynamics.

The difference in the dynamics for the two simulations is also illustrated by the dynamics of the HDNB conformers, whose PES is illustrated in Figure 3. For the thermal simulations, with random sampling of the HDNB initial conditions, there is statistical sampling of the HDNB conformations before reaction occurs. However, for the H• + •DNB association dynamics studied here, there is not statistical sampling of the HDNB conformers before the observed reaction products are formed. Only for the trajectories that form a HDNB intermediate, that does not react within the 1 ps trajectory simulations, are there transitions between the HDNB conformers.

6. SUMMARY

Eight reaction pathways are found in a direct dynamics simulation modeling H^+ + DNB^- collisions. Possible formation of the highly vibrationally excited HDNB molecule is modeled by assuming an electronic transition from the H^+ + DNB^- to H• + •DNB PES and simulating the collisions on this latter surface. The most likely event, that is, 2/3 of the trajectories, is for the H-atom to directly scatter off of •DNB without forming a "hot" HDNB molecule. For most of the trajectories, an insufficient amount of the H• + •DNB relative translational energy is transferred to •DNB vibrational energy to form a vibrationally excited HDNB molecule. Another way to view these dynamics is that there is insufficient IVR from the incipient H−DNB bond of the H• + •DNB collision to other vibrational modes, and the H• atom directly scatters from •DNB.

Approximately 1/4 of the trajectories followed path 2 in Table 3, forming the $H_2N_2O_2$ product, which has an isomerization pathway to HNNOOH. The $H_2N_2O_2$/HNNOOH product pathway may undergo seven different secondary dissociations. This reaction occurs by the colliding H-atom first interacting with the central N-atom and the two adjacent O-atoms of •DNB, which is then followed by IVR promoting the chemical reaction. This was found to also be an important pathway for HDNB dissociation in a previous direct dynamics simulation by Liu et al.,[14] for which HDNB was thermally excited.

In summary, a comparison of the current results with the previous study by Liu et al.[14] shows that the initial conditions for the excited HDNB moiety are crucial for its ensuing unimolecular dynamics. H^+ + DNB^- association localizes the energy in HDNB, creating a "hot spot", and IVR is not sufficiently rapid to give the unimolecular dynamics found by Liu et al. for their random, thermal initial conditions. For this previous simulation, there were rapid statistical, interconversions between all of the HDNB conformers before unimolecular dissociation occurred. In future work, it would be of interest to study both the random and nonrandom excitation of HDNB in a condensed-phase liquid environment.

■ ASSOCIATED CONTENT

Supporting Information

A trajectory (mpg file) shows the interconversion of various HDNB conformers. This material is available free of charge via the Internet at http://pubs.acs.org.

■ AUTHOR INFORMATION

Corresponding Authors

*E-mail: steven.chambreau.ctr@us.af.mil.
*E-mail: Jianbo.Liu@qc.cuny.edu. Phone: (718) 997-3271.
*E-mail: bill.hase@ttu.edu. Phone: (806)-834-3152.

Present Address

#M.R.S.: Department of Chemistry, Missouri State University, 901 S National Ave, Springfield, MO 65897.

Notes

The authors declare no competing financial interest.

■ ACKNOWLEDGMENTS

This material is based upon work supported by the Air Force Office of Scientific Research under Contract FA9550-11-C-0020, the Robert A. Welch Foundation under Grant D-0005, and the National Science Foundation under Grant CHE-0957521. J.L. acknowledges the financial support received from the Air Force Research Laboratory and the partial support from the National Science Foundation Career Award under Grant CHE-0954507. S.D.C. and G.L.V. gratefully acknowledge funding from the U.S. Air Force Office of Scientific Research (Grant FA9300-06-C-0023). Support was also provided by the High-Performance Computing Center (HPCC) at Texas Tech University, under the direction of Philip W. Smith, the Texas Advanced Computing Center (TACC) at the University of Texas at Austin, and the TTU Department of Chemistry & Biochemistry cluster Robinson, whose purchase was funded by the National Science Foundation under the CRIF-MU Grant No. CHE-0840493.

■ REFERENCES

(1) Sutton, G. P.; Oscar, B. *Rocket Propulsion Elements*, 7th ed.; John Wiley & Sons, Inc.: New York, 2001.

(2) Kelkar, M. S.; Maginn, E. J. *J. Phys. Chem. B* **2007**, *111*, 9424−9427.

(3) Smiglak, M.; Metelen, A.; Rogers, R. D. *Acc. Chem. Res.* **2007**, *40*, 1182−1192, and references therein.

(4) Rogers, R. D.; Voth, G. A. *Acc. Chem. Res.* **2007**, *41*, 1077−1078, and articles therein on the special issue "Ionic Liquids".

(5) Wishart, J. F.; Castner, E. W. *J. Phys. Chem. B* **2007**, *111*, 4639−4640, and articles therein on the special issue "The Physical Chemistry of Ionic Liquids".
(6) Yoshida, Y.; Muroi, K.; Otsuka, A.; Saito, G.; Takahashi, M.; Yoko, T. *Inorg. Chem.* **2004**, *43*, 1458−1462.
(7) MacFarlane, D. R.; Golding, J.; Forsyth, S.; Forsyth, M.; Deacon, G. B. *Chem. Commun.* **2001**, *16*, 1430−1431.
(8) Laus, G.; Bentivoglio, G.; Schottenberger, H.; Kahlenberg, V.; Kopacka, H.; Roeder, H.; Roeder, T.; Sixta, H. *Lenzinger Ber.* **2005**, *84*, 71−85.
(9) Schneider, S.; Hawkins, T.; Rosander, M.; Vaghjiani, G.; Chambreau, S.; Drake, G. *Energy Fuels* **2008**, *22*, 2871−2872.
(10) Chambreau, S. D.; Schneider, S.; Rosander, M.; Hawkins, T.; Gallegos, C. J.; Pastewait, M. F.; Vaghjiani, G. L. *J. Phys. Chem. A* **2008**, *112*, 7816−7824.
(11) Izgorodina, E. I.; Chesman, A. S. R.; Turner, D. R.; Deacon, G. B.; Batten, S. R. *J. Phys. Chem. B* **2010**, *114*, 16517−16527.
(12) Lourderaj, U.; Park, K.; Hase, W. L. *Int. Rev. Phys. Chem.* **2008**, *27*, 361−403.
(13) Sun, L.; Hase, W. L. *Rev. Comput. Chem.* **2003**, *19*, 79−146.
(14) Liu, J.; Chambreau, S. D.; Vaghjiani, G. L. *J. Phys. Chem. A* **2011**, *115*, 8064−8072.
(15) *NIST Chemistry WebBook*. http://webbook.nist.gov/chemistry/ (2011).
(16) Izgorodina, E. I.; Bernard, U. L.; MacFarlane, D. R. *J. Phys. Chem. A* **2009**, *113*, 7064−7072.
(17) Zhao, Y.; Truhlar, D. G. *J. Chem. Theory Comput.* **2006**, *2*, 1009−1018.
(18) Zhao, Y.; Schultz, N. E.; Truhlar, D. G. *J. Chem. Theory Comput.* **2006**, *2*, 364−382.
(19) Aikens, C. M.; Webb, S. P.; Bell, R. L.; Fletcher, G. D.; Schmidt, M. W.; Gordon, M. S. *Theor. Chem. Acc.* **2003**, *110*, 233−253.
(20) Hehre, W. J.; Ditchfield, R.; Pople, J. A. *J. Chem. Phys.* **1972**, *56*, 2257−2261.
(21) Krishnan, R.; Binkley, J. S.; Seeger, R.; Pople, J. A. *J. Chem. Phys.* **1980**, *72*, 650−654.
(22) Dunning, T. H., Jr. *J. Chem. Phys.* **1989**, *90*, 1007−1023.
(23) Kendall, R. A.; Dunning, T. H., Jr.; Harrison, R. J. *J. Chem. Phys.* **1992**, *96*, 6796−6806.
(24) Becke, A. D. *J. Chem. Phys.* **1993**, *98*, 5648−5652.
(25) Frisch, A. E.; Frisch, M. J.; Trucks, G.; et al. *Gaussian 03*, User's Reference; Gaussian, Inc.: Pittsburgh, PA, 2003.
(26) Adamo, C.; Barone, V. *J. Chem. Phys.* **1999**, *110*, 6158−6170.
(27) Becke, A. D. *Phys. Rev. A* **1988**, *38*, 3098−3100.
(28) Lee, C.; Yang, W.; Parr, R. G. *Phys. Rev. B* **1988**, *37*, 785−789.
(29) Becke, A. D. *J. Chem. Phys.* **1996**, *104*, 1040−1046.
(30) Xu, X.; Goddard, W. A., III. *Proc. Natl. Acad. Sci. U.S.A.* **2004**, *101*, 2673−2677.
(31) Slater, J. C. *The Self-Consistent Field for Molecular and Solids, Quantum Theory of Molecular and Solids*; McGraw-Hill: New York, 1974; Vol. *4*.
(32) Vosko, S. H.; Wilk, L.; Nusair, M. *Can. J. Phys.* **1980**, *58*, 1200−1211.
(33) Raghavachari, K.; Trucks, G. W.; Pople, J. A.; Head-Gordon, M. *Chem. Phys. Lett.* **1989**, *157*, 479−483.
(34) Hase, W. L.; Duchovic, R. J.; Hu, X.; Komornicki, A.; Lim, K. F.; Lu, D. H.; Peslherbe, G. H.; Swamy, S. R.; Vande Linde, S. R.; Varandas, A.; et al. *Quantum Chem. Program Exchange Bull.* **1996**, *16*, 671.
(35) Hu, X.; Hase, W. L.; Pirraglia, T. *J. Comput. Chem.* **1991**, *12*, 1014−1024.
(36) Lourderaj, U.; Sun, R.; Swapnil, C. K.; Barnes, G. L.; de Jong, W. A.; Windus, T. L.; Hase, W. L. *Comput. Phys. Commun.* **2014**, *185*, 1074−1080.
(37) Valiev, M.; Bylaska, E. J.; Govind, N.; Kowalski, K.; Straatsma, T. P.; van Dam, H. J. J.; Wang, D.; Nieplocha, J.; Apra, E.; Windus, T. L.; et al. *Comput. Phys. Commun.* **2010**, *181*, 1477−1489.
(38) Peslherbe, G. H.; Wang, H.; Hase, W. L. *Adv. Chem. Phys.* **1995**, *105*, 171−202.
(39) Swope, W. C.; Anderson, H. C.; Berens, P. H.; Wilson, K. R. *J. Chem. Phys.* **1982**, *76*, 637−649.
(40) Schlier, C.; Seiter, A. *Comput. Phys. Commun.* **2000**, *130*, 176−189.
(41) Schlier, C.; Seiter, A. *J. Phys. Chem. A* **1998**, *102*, 9399−9404.
(42) Marcus, R. A. *J. Chem. Phys.* **1952**, *20*, 359−364.